J. Fluid Mech. (1990), *vol.* 213, *pp.* 377–396
Printed in Great Britain

Unsteady three-dimensional natural convection in a fluid-saturated porous medium

By DOUGLAS W. STAMPS†, VEDAT S. ARPACI AND JOHN A. CLARK

Department of Mechanical Engineering and Applied Mechanics, University of Michigan, Ann Arbor, MI 48109, USA

(Received 9 December 1985 and in revised form 19 July 1989)

Natural convection in a cube of fluid-saturated porous medium having a constant temperature top and bottom is studied numerically. In the first of two special cases considered, the vertical sides are insulated. In this case, the numerical simulations indicate permanently unsteady regularly and irregularly fluctuating convective states at Rayleigh numbers (R^*) above 550. The regularly fluctuating convective state defined by simply periodic oscillations in the Nusselt number begins at R^* between 550 and 560. The frequency of the oscillations appears to depend on R^* approximately as $f \propto (R^*)^{3.6}$. The irregularly fluctuating convective state defined by random variations in the Nusselt number begins at R^* between 625 and 640. In the second case, heat is transferred through the vertical sides of the cube. Three distinct flow patterns are identified depending on the rate of heat transfer and the Rayleigh number. For all runs in the range of Rayleigh numbers studied, the transition from the first to the second flow pattern occurs abruptly.

1. Introduction

According to linear theory, Beck (1972) shows that convection begins in a cube of porous medium with isothermal top and bottom and insulated vertical sides when the Rayleigh number, R^*, equals $4\pi^2$. A two-dimensional roll cell is the only stable pattern immediately above the critical R^* value. At $R^* = 4.5\pi^2$, a three-dimensional convective mode begins with an ascending flow at diagonally opposed edges of the cube and a descending flow at the other diagonally opposed edges. Using an analytic eigenfunction-expansion technique, Steen (1983) shows the stabilization of this three-dimensional convective mode for $R^* > 4.87\pi^2 = 48.06$. Above this value of R^*, both two- and three-dimensional flows may exist.

It was proposed by Malkus (1954) and Platzman (1965) that the type of flow (either two- or three-dimensional) that evolves to a steady configuration will maximize the heat transport. However, Straus & Schubert (1979) find numerically that both types of flow exist in a cube even though two-dimensional flows transport more heat than three-dimensional ones do for $R^* \leqslant 97$, while the opposite is true for $R^* \geqslant 97$. This is verified by Holst & Aziz (1972) who calculate both two- and three-dimensional flows in cubes at $R^* = 60$ and 120. Although two-dimensional or three-dimensional convection cannot be predicted based on the flow that maximizes the heat transport, Schubert & Straus (1979) find it is possible to force a specific type of flow by emphasizing a particular mode in the initial conditions. On the other hand,

† Current address: Innovative Technology Applications Division, Sandia National Laboratories, Albuquerque, NM 87185.

different sets of random initial conditions give either two- or three-dimensional convection for the same R^* value. Steen (1983) obtains the regions within the space of initial conditions that lead to one or the other of these competing flows. Once the type of flow is established based on initial conditions, both two- and three-dimensional flows are steady for R^* above the critical. The flow remains steady until a second critical R^* is attained. The flow changes from steady convection to regularly fluctuating convection above the second critical R^*.

Using a Galerkin method, Schubert & Straus (1979) find the onset of the three-dimensional regularly fluctuating convective state in a cube of porous medium to occur at R^* between approximately 300 and 320. At larger R^*,the flow changes from regularly fluctuating to irregularly fluctuating convection. The three-dimensional irregularly fluctuating convective state begins at R^* between 350 and 400 and exists to the largest value computed at $R^* = 500$. Horne (1979) is the only other investigator to observe time-dependent three-dimensional convection in a cube of porous medium. The flow is largely a two-dimensional roll with 'waves' moving in the third dimension. Using finite-differencing schemes, he observes irregular fluctuations at $R^* = 300$ and 400. The values obtained numerically for the onset of three-dimensional fluctuating convection have not been verified experimentally. To the authors' knowledge, no experimental data have been reported for fluctuating convection in a cube of porous medium.

The only experimental verification of fluctuating convection in a three-dimensional geometry is in two concentric horizontal cylinders. In this experiment, Caltigirone (1976) uses a visual technique to observe a three-dimensional thermal field for $R^* > 70$ in the upper part of the annular layer. Since the cell for visualization did not yield precise information on the heat transfer between the cylinders, Caltigirone constructed another experimental cell with thermocouples placed in the fluid saturating the porous material. For $R^* > 65$, the flow changes from steady two-dimensional convection to fluctuating three-dimensional convection in the upper part of the annular layer as evidenced by fluctuations in the fluid temperature.

Other experimental studies verify the existence of the fluctuating convective state in fluid-saturated porous media having different geometries. These geometries are categorized into two groups. The first includes geometries that have a vertical length much smaller than either horizontal length and are referred to as horizontal layers. The second group includes geometries that have one horizontal length much smaller than the other horizontal and vertical lengths. The essentially two-dimensional flows that exist in these geometries approximate the motion in the cross-section of an infinite horizontal rectangular channel that contains a strictly two-dimensional roll. These geometries are referred to as rectangular cross-sections.

The fluctuating convective state is observed experimentally to exist in both horizontal layers and rectangular cross-sections. Combarnous & LeFur (1969) observe the fluctuating convective state in a horizontal layer and a more detailed description is given later by Combarnous (1970). The fluctuating convection begins in the range $240 < R^* < 390$ and the onset depends on the characteristics of the porous medium. An abrupt change in the slope of the Nusselt–Rayleigh number (Nu–R^*) curve occurs at the onset of the fluctuating convection. Gupta & Joseph (1973) compute the theoretical bounding heat-transport (Nu–R^*) curve for natural convection in an infinite horizontal layer of porous medium using a variational method. Their results indicate that the slope of the Nu–R^* curve changes at $R^* = 221.5$. Their value compares well with the experimental value $R^* = 245$ that Buretta & Berman (1976) obtain for the change in slope of their Nu–R^* curve. Using a

Investigator	Critical Rayleigh number	Nusselt number	Period of oscillation
Horne & O'Sullivan (1974)	280	NA	0.029
Caltagirone (1975)	384 ± 5	NA	NA
Schubert & Straus (1979, 1982)	380–400	5.09–5.45	0.012
Gary & Kassoy (1981)	350–400	4.99–5.07	0.01175

TABLE 1. Comparison of the critical Rayleigh number at the onset of fluctuating convection for two-dimensional flow in a square cross-section. The comparisons between the minimum and maximum Nusselt numbers and the non-dimensional time period between succeeding Nusselt maxima are for the case $R^* = 400$.

horizontal layer, Seki, Fukusako & Ariake (1980) find that the fluctuating convection begins in the range $260 < R^* < 320$ and is dependent on the characteristics of the porous medium. They observe both regular and irregular fluctuations in the fluid temperature although the value of R^* at which the irregular fluctuations begin is not reported. They also observe that the frequency of the oscillations in the fluid temperature for the regularly fluctuating convection increases with increasing R^* values. Caltagirone, Clopeau & Combarnous (1971) observe experimentally that fluctuating convection begins in the range $190 < R^* < 390$ for a rectangular cross-section.

In addition to Caltagirone's experimental work using a rectangular cross-section, there are several numerical investigations on two-dimensional fluctuating convection in a square cross-section of porous medium with the top and bottom at a constant temperature and insulated sides. A comparison of the value of R^* at the onset of regularly fluctuating single-cell convection is summarized in table 1. Also the range from the minimum to the maximum Nusselt number and the period between succeeding Nusselt maxima are listed for the case $R^* = 400$. The value of R^* for the onset of regularly fluctuating convection is generally higher in rectangular cross-sections than horizontal layers. This is due possibly to the stabilizing effect of the lateral walls. Schubert & Straus (1982) suggest possible forms for a functional relationship between the frequency f of the oscillations in the Nusselt number and R^*. They observe three regimes in regularly fluctuating two-dimensional convection: in the first regime, $f \propto (R^*)^{\frac{7}{8}}$, the second regime is characterized by two frequencies, and in the third regime, $f \propto (R^*)^{\frac{3}{2}}$. In the range of two-dimensional flows computed, Horne & O'Sullivan (1978) also observe that $f \propto (R^*)^{\frac{3}{2}}$.

Although none of the works mentioned earlier include heat transfer through the vertical sides, variations in the boundary conditions can have large effects on the natural convective motion in porous media. The mathematical convenience of perfectly insulated sides may not be realistic in many practical applications. Stamps & Clark (1986) find it necessary to include finite heat transfer at the boundaries of a rectangular volume of porous medium to predict numerically the unsteady thermocline degradation in a solar thermal storage device. Recognition of finite heat transfer rates at the boundaries is shown to be a significant factor in improving the predictive capability of the numerical model. Further, different flow patterns exist for boundaries with finite heat transfer and insulated boundaries. The phenomenon of boundary-affected flows has also been observed by Kassoy & Cotte (1985) for the onset of convection in a thin, vertically oriented, finite slab of porous medium with

sidewall heat transfer. Lowell & Hernandez (1982) include the effect of boundary conditions on finite-amplitude convection in a similar geometry.

Although these studies demonstrate the importance of boundary-affected flows, none address the question of how much heat transfer is necessary to produce the different flows that may exist. Additionally, the question of whether the transition among the different flows is continuous or abrupt has not been addressed. Riahi (1983) considers the first question for a horizontal layer with finite conducting boundaries. He finds that three-dimensional square-flow-pattern convection and two-dimensional rolls may exist at the onset of convection, depending on a fixed set of values of the thermal conductivity of the fluid and the upper and lower boundaries. Weidman & Kassoy (1986) find that two- and three-dimensional flows may exist at the onset of convection in a thin, vertically oriented, finite slab of porous medium depending on the rate of heat transfer from the vertical sides. The problem of boundary-affected flows and the nature of the transition among these flows has not been considered for boxes.

In summary, additional work at high Rayleigh numbers is necessary to describe the permanently unsteady fluctuating convective state in a cube of porous medium with constant temperature top and bottom and insulated vertical sides. Schubert & Straus (1979) consider this problem and perform calculations up to $R^* = 500$. The first of the two objectives in the present investigation is to extend the calculations to $R^* = 800$. In a related problem, the effect of finite heat transfer at the boundaries of a porous medium is considered. No study has considered boundary-affected flows in rectangular boxes. The second objective in the present investigation is to describe the motion in a cubic box of porous medium resulting from variations in the boundary conditions. The results indicate that both two- and three-dimensional motion exist, depending on the rate of heat transfer through the vertical sides and the Rayleigh number. This objective includes identifying the types of flow pattern that exist and the nature of the transitions among flow patterns.

2. Formulation and solution

Consider a rectangular volume of a fluid-saturated homogeneous and isotropic porous medium with impermeable sides and finite heat transfer on all sides. The bottom of the volume is $z = 0$ and the top is $z = L_z$. The sides of the volume are $x = 0, x = L_x, y = 0$, and $y = L_y$. Although the equations are developed for a volume with arbitrary dimensions and arbitrary thermal boundary conditions, the present numerical results are restricted to a cube with constant temperature top and bottom.

The following assumptions are inherent in the derivation of equations (1)–(3) below: (i) all properties are constant except for variations in the density with temperature in the body force term, (ii) the fluid density is a linear function of the temperature, (iii) inertial effects are negligible, (iv) thermal dispersion is negligible, and (v) the fluid and solid are in local thermal equilibrium. The non-dimensional volume-averaged equations governing convection in a volume of porous medium are the conservation of mass, momentum (Darcy's law), and energy:

$$\nabla \cdot V = 0, \tag{1}$$

$$V = -\nabla p_T + R^* T \boldsymbol{k}, \tag{2}$$

$$\frac{\partial T}{\partial t} + V \cdot \nabla T = \nabla^2 T, \tag{3}$$

where $R^* \equiv \beta(T_\ell - T_u)\, gKL_x/\nu_f \alpha_m$ is the modified Rayleigh number for porous media. In this dimensionless number, β is the thermal coefficient of volume expansion, T_ℓ and T_u are respectively the initial lower and upper surface temperatures along a vertical line at the centre of the volume, g is the acceleration due to gravity, K is the permeability of the medium, ν_f is the kinematic viscosity of the fluid, and α_m is the thermal diffusivity of the saturated porous medium. The thermal diffusivity is defined as $\alpha_m = k_m^*/(\rho c_p)_f$, where k_m^* is the effective thermal conductivity of the fluid and solid matrix. In the governing equations, V is the Darcy velocity, p_T is the dynamic pressure, T is the temperature, and $\boldsymbol{k}$ is a unit vector in the positive z-direction. Equations (1)–(3) are non-dimensionalized by letting $(x', y', z') = L_x(x, y, z)$,

$$V' = \frac{\alpha_m}{L_x} V, \quad p'_T = \frac{\alpha_f \mu}{K} p_T, \quad t' = \frac{(\rho c_p)_m L_x^2 t}{k_m^*}, \quad T = \frac{T' - T_u}{T_\ell - T_u}$$

where the primes denote dimensional quantities. Unless otherwise specified, the subscripts f and m denote fluid and porous medium respectively.

Horne (1979) shows that by introducing a vector potential of the form

$$\boldsymbol{V} = \boldsymbol{\nabla} \times \boldsymbol{\Phi} \tag{4}$$

into the formulation, the resulting equations may be solved numerically faster and more accurately than with the formulation using the primary variables in (1) and (2). This vector potential satisfies identically the continuity equation. Hirasaki & Hellums (1968) show that the potential is also solenoidal since the velocity is solenoidal:

$$\boldsymbol{\nabla} \cdot \boldsymbol{\Phi} = 0. \tag{5}$$

Introducing (4) and (5) into the curl of (2) yields the following set of equations:

$$\nabla^2 \Phi_x = -R^* \frac{\partial T}{\partial y}, \tag{6}$$

$$\nabla^2 \Phi_y = R^* \frac{\partial T}{\partial x}, \tag{7}$$

$$\nabla^2 \Phi_z = 0. \tag{8}$$

For rigid boundaries, the boundary conditions in terms of the vector potential are derived by Hirasaki & Hellums (1968):

$$\Phi_x = \Phi_y = \frac{\partial \Phi_z}{\partial z} = 0 \quad \text{at} \quad z = 0, \frac{L_z}{L_x}; \tag{9}$$

$$\Phi_x = \frac{\partial \Phi_y}{\partial y} = \Phi_z = 0 \quad \text{at} \quad y = 0, \frac{L_y}{L_x}; \tag{10}$$

$$\frac{\partial \Phi_x}{\partial x} = \Phi_y = \Phi_z = 0 \quad \text{at} \quad x = 0, 1. \tag{11}$$

The solution to (8) using the boundary conditions for Φ_z is $\Phi_z = 0$ everywhere.

The non-dimensional thermal boundary conditions are

$$\frac{\partial T}{\partial z} \pm B^*(T - T_\infty) = 0 \quad \text{at} \quad z = 0, \frac{L_z}{L_x}; \tag{12}$$

$$\frac{\partial T}{\partial y} \pm B^*(T - T_\infty) = 0 \quad \text{at} \quad y = 0, \frac{L_y}{L_x}; \tag{13}$$

$$\frac{\partial T}{\partial x} \pm B^*(T - T_\infty) = 0 \quad \text{at} \quad x = 0, 1. \tag{14}$$

The minus sign corresponds to the boundary at the origin and the plus sign corresponds to the other boundary. The dimensionless ratio B^* is a modified Biot number for porous media and is defined as $B^* \equiv hL_x/k_m^*$, h being the heat transfer coefficient on the outside of the volume and T_∞ the ambient temperature. For the numerical results presented in this study, the top and bottom are at $T = 0$ and 1 respectively and $B^* \to \infty$. For insulated vertical sides, $B^* = 0$.

The parabolic part of the formulation (3) is solved using the alternating directions implicit (ADI) method and the elliptic part corresponding to (6) and (7) is solved using the successive line over-relaxation method. These methods are described in Roache (1972). Both methods are fully implicit and are second-order accurate in space even at the boundaries. The ADI method is also second-order accurate in time. The full second-order accuracy of the ADI method can be deteriorated by the nonlinear terms in the energy equation unless the values of the velocity terms are at the current intermediate time step. This requires an iterative process, and a minimum of three iterations within each time step is performed in this study. A detailed derivation of the governing equations and description of the solution method is given by Stamps (1985).

3. Results

3.1. *Natural convection in a cube with insulated vertical sides*

All results are obtained for a cube with constant temperature top and bottom and insulated vertical sides. In this problem, as the Rayleigh number increases, at least four distinct regimes are identified for three-dimensional natural convection including a conduction, a steady convection, a permanently unsteady regularly fluctuating convection, and a permanently unsteady irregularly fluctuating convection regime. These results agree with the four regimes observed by Schubert & Straus (1979) for the same geometry and boundary conditions. The same four regimes have also been observed experimentally in a horizontal layer by Seki *et al.* (1980) and numerically in a square cross-section by Schubert & Straus (1979).

Table 2 summarizes the results for the steady convection regime. Nu is the instantaneous Nusselt number spatially averaged over the bottom plane and N, M, and P are the number of grid points in the x-, y-, and z-directions respectively. The Nusselt number is constant to at least five significant figures in the steady convection regime. Odd grid sizes are used because the Rayleigh number is calculated initially along the vertical centreline of the cube. The results of the present investigation indicate that convection begins at $R^* = 4\pi^2$ which verifies Beck's (1972) results for the onset of convection in a cube. For $4\pi^2 \leqslant R^* \leqslant 300$, the Nusselt numbers obtained in the present investigation agree to within less than 1% with those obtained by Schubert & Straus (1979). For $320 \leqslant R^* \leqslant 500$, Schubert & Straus obtain fluctuating

Rayleigh number (R^*)	Nusselt number (Nu)	Grid size ($N \times M \times P$)
39.48 ($4\pi^2$)	1.00	$9 \times 9 \times 33$
50	1.16	$9 \times 9 \times 33$
100	2.66	$9 \times 9 \times 33$
150	3.69	$9 \times 9 \times 33$
200	4.48	$9 \times 9 \times 33$
250	5.11	$9 \times 9 \times 33$
300	5.66	$11 \times 11 \times 41$
400	6.41	$29 \times 29 \times 29$
550	7.25	$29 \times 29 \times 29$

TABLE 2. Nusselt numbers for steady natural convection in a cube of porous medium. N, M, and P are the number of grid points in the x-, y-, and z-directions, respectively.

R^*	$\overline{Nu}$	Nu_{max}–Nu_{min}	τ_p
560	7.30	7.303–7.296	0.0055
580	7.43	7.46–7.39	0.0053
600	7.71	7.78–7.64	0.0046
625	8.02	8.06–7.98	0.0038
640	8.44	8.64–8.22	0.0027–0.0066
650	8.58	8.95–8.31	0.0024–0.0072
700	9.80	10.44–9.20	0.0016–0.0084
800	10.84	11.59–10.11	0.0012–0.0072

TABLE 3. Nusselt numbers for unsteady natural convection in a cube of porous medium. $\overline{Nu}$ is the time-averaged value, Nu_{max} and Nu_{min} are the largest and smallest values in the run respectively, and τ_p is the time period between successive maxima. All values are calculated using a grid size of $N \times M \times P = 29 \times 29 \times 29$.

convection, and since they do not report time-averaged Nusselt numbers no direct comparison can be made.

The results of the fluctuating convection regimes are summarized in table 3. The time-averaged Nusselt number, $\overline{Nu}$, is defined as

$$\overline{Nu} = \frac{1}{t_{total}} \sum_{t=1}^{t_{max}} Nu(t)\,\Delta t,$$

where $Nu(t)$ is the instantaneous spatially averaged Nusselt number, Δt is the time step, t_{max} is the maximum number of time steps considered, and t_{total} is the total time period. The range of Nusselt number, $Nu_{max} - Nu_{min}$, is the difference between the largest and smallest values in the run and τ_p is the time period between successive Nusselt maxima.

Regularly fluctuating convection begins in a cube at R^* between 550 and 560. This differs from the only other value for the onset of fluctuating convection in a cube which Schubert & Straus (1979) determine using a Galerkin method to be between $300 < R^* < 320$. Their final steady Nusselt value $Nu = 5.642$ at $R^* = 300$ calculated with a truncation level $N = 14$ compares quite well with the value $Nu = 5.658$ at $R^* = 300$ in the present study using 4961 grid points ($11 \times 11 \times 41$). They use a less

accurate truncation level, $N = 12$, to determine the onset of fluctuating convection at $R^* = 320$. In contrast, the present study determines the onset of fluctuating convection using 24389 grid points ($29 \times 29 \times 29$). Additionally Schubert & Straus use a first-order-accurate explicit time-stepping procedure compared with the second-order-accurate implicit temporal method used in the present study.

The transition Rayleigh number asymptotically approaches a limiting value as the spatial resolution increases. The transition number for an $11 \times 11 \times 11$ grid (1331 grid points) is $380 < R^* < 400$. As the grid size is increased to $17 \times 17 \times 17$ (4913 grid points), the transition Rayleigh number increases to $470 < R^* < 485$. Using a $23 \times 23 \times 23$ grid (12167 grid points), the transition number is $530 < R^* < 540$. By approximately doubling the number of grid points relative to the $17 \times 17 \times 17$ grid, the transition number increases by about 60. If the number of grid points is doubled again with a $29 \times 29 \times 29$ grid (24389 grid points), the transition number increases asymptotically to $550 < R^* < 560$. The slight increase of 20 in the transition Rayleigh number as the grid is increased from $23 \times 23 \times 23$ to $29 \times 29 \times 29$ is within the level of accuracy of the transition number generally reported for a given grid size. For example, Schubert & Straus (1979) determine their transition number to be $300 < R^* < 320$.

It is not unreasonable to expect a larger Rayleigh number than Schubert & Straus obtained for the onset of fluctuating convection for two reasons. First, in a two-dimensional problem similar to the current one, Schubert & Straus (1979, 1982) determine that the value of the transition Rayleigh number between steady and fluctuating convection increases with increasing accuracy of the solution. They find that by increasing the level of truncation from $N = 10$ to $N = 18$, the transition Rayleigh number increases from $300 < R^* < 320$ to $380 < R^* < 400$. For the second reason, higher transition Rayleigh numbers are expected for cubic boxes than less confined geometries. Seki *et al.* (1980) report a transition Rayleigh number in the range $260 < R^* < 320$ for a horizontal layer while Schubert & Straus (1982) report a larger value $380 < R^* < 400$ in a square cross-section. It is reasonable to expect that an even larger transition Rayleigh number, such as the $550 < R^* < 560$ obtained in the present study, should occur in a cubic box than in either a square cross-section or a horizontal layer because of the stabilizing effect of the lateral walls.

Horne (1979) is the only other investigator to obtain time-dependent convection in a cube; however, his results cannot be compared with the present results since his flows are essentially two-dimensional. Horne's initial (1, 1, 0.1) modal disturbance for his $R^* = 300$ and 400 runs evolves largely into an overall two-dimensional flow with 'waves' moving in the third dimension. This flow is unlike the three-dimensional flows that evolve from the initial (1, 1, 1) modal disturbances used in the present investigation and that of Schubert & Straus (1979). Horne solves the energy equation using a first-order-accurate explicit forward time-stepping procedure, a fourth-order Arakawa template for the advection terms, and a $17 \times 17 \times 17$ grid for his two time-dependent runs at $R^* = 300$ and 400. This compares to the second-order-accurate implicit temporal and spatial methods and a $29 \times 29 \times 29$ grid used for the time-dependent runs in the present investigation.

From table 3 it is seen that in the regularly fluctuating convection, $560 \leqslant R^* \leqslant 625$, the period τ_p decreases, or frequency f increases, with increasing Rayleigh number. This relationship between f and R^* has not been observed previously in natural convective flows in rectangular boxes. However, Seki *et al.* (1980) and Schubert & Straus (1982) observe this numerically in a square cross-section. Irregularly fluctuating convection begins in a cube at R^* between 625 and 640. The

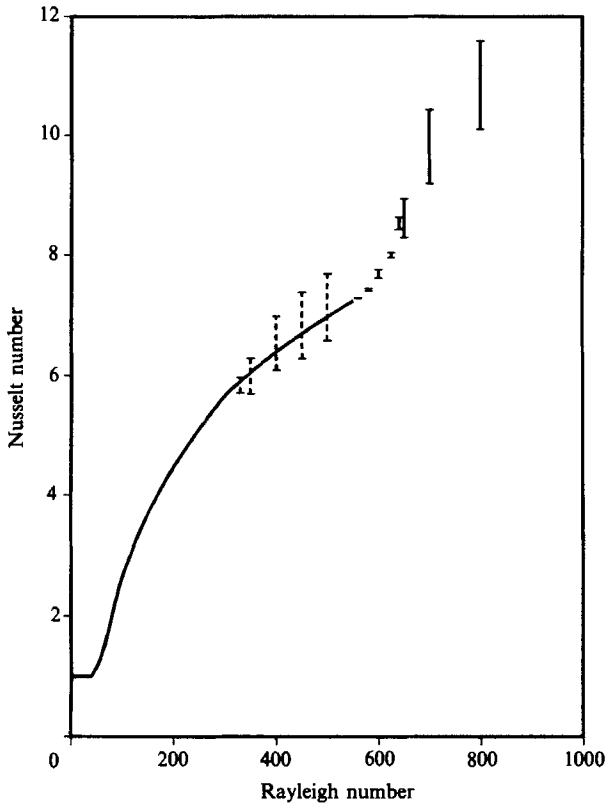

FIGURE 1. The Nusselt number as a function of the Rayleigh number for three-dimensional convection in a cube having insulated vertical sides and constant temperature top and bottom. The solid line represents the Nusselt numbers in the steady convection regime. The solid and dashed crossbars represent the range between the minimum and maximum Nusselt numbers in the unsteady convection regime for the present investigation and Schubert & Straus (1979), respectively.

nature of this flow is characterized by a Nusselt number that is composed of either two basic frequencies or random variations that are not composed of any distinct frequencies. This compares to the range $350 < R^* < 400$ that Schubert & Straus (1979) obtain for the same geometry and boundary conditions. When a range is given for the period rather than a single value for $640 < R^* < 800$, it indicates that the period is observed to vary over that range. It can be seen from table 3 that the range of τ_p increases with increasing Rayleigh number. These results agree with those Schubert & Straus (1979) obtain. The time step used for all runs is always an order of magnitude less than the average time period.

The Nusselt numbers reported for the current grid sizes vary by less than 1 % from the Nusselt numbers at the next smaller grid size. The accuracy in the Nusselt number applies to the steady-state results listed in table 2 as well as the time-dependent results listed in table 3. In the time-dependent cases, the time-averaged Nusselt number is used. As an example, for the largest Rayleigh number run at $R^* = 800$ the time-averaged Nusselt number $\overline{Nu} = 10.84$ for the grid size of $N \times M \times P = 29 \times 29 \times 29$ varies by less than 1 % from the value $\overline{Nu} = 10.75$ at the next smaller grid size of $N \times M \times P = 27 \times 27 \times 27$. Additionally, the range of time period values remains the same for $R^* = 800$ for these two different grid sizes. As an example of a

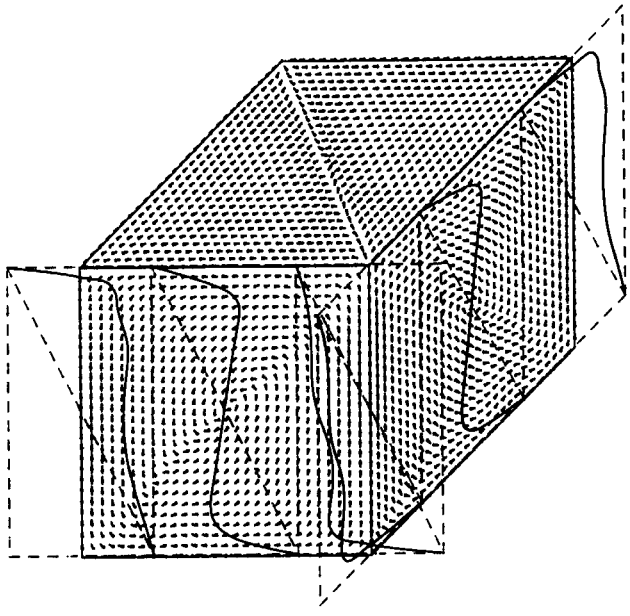

FIGURE 2. Velocity and temperature distributions at the boundaries of a cube with insulated vertical sides for $R^* = 600$ at the time $t = 0.3471$ corresponding to a local Nusselt minimum. The grid size is $29 \times 29 \times 29$. Arrows represent velocity vectors and solid lines represent vertical temperature distributions at the centre and corners of the vertical sides.

steady-state case, at $R^* = 300$ the Nusselt number $Nu = 5.66$ for the grid size of $N \times M \times P = 11 \times 11 \times 41$ varies by less than 1% from the value $Nu = 5.62$ at the next smaller grid size of $N \times M \times P = 9 \times 9 \times 33$.

The four regimes may be summarized in the Nusselt–Rayleigh (Nu–R^*) curve shown in figure 1. The abrupt change in the slope of the curve at approximately $R^* = 40$ marks the transition between the conduction regime and the steady convection regime. Steady convection is represented by a solid line that is obtained by a cubic-spline fit of the data in table 2. Unsteady convection is represented by the values of the time-averaged Nusselt number in table 3 with the solid cross bars marking the range between the minimum and maximum Nusselt numbers. The values of the Nusselt number in the unsteady convection regime do not lie on a smooth extension of the steady convection curve. The change in the slope of the curve between $R^* = 550$ and 560 marks the transition between steady and unsteady convection. Combarnous (1970) and Buretta & Berman (1976) observe experimentally an abrupt change in the slope of their Nu–R^* curve between steady and unsteady convection in a horizontal layer. The results Schubert & Straus (1979) obtain for a cube are included in figure 1. Since their values for $4\pi^2 < R^* < 300$ are nearly identical to the values of the present study, the points coincide on the same curve. They obtain fluctuating convection for $320 < R^* < 500$ and the dashed cross bars represent the range between the minimum and maximum Nusselt numbers.

The case $R^* = 600$ is used to demonstrate typical flow patterns and temperature distributions for the regularly fluctuating convection regime as shown in figure 2. The arrows represent the velocity vectors on the cube faces. Note that the volume-averaged governing equations for porous media allow for slip on rigid walls. The length of the arrow corresponds to the magnitude of the velocity. The three solid

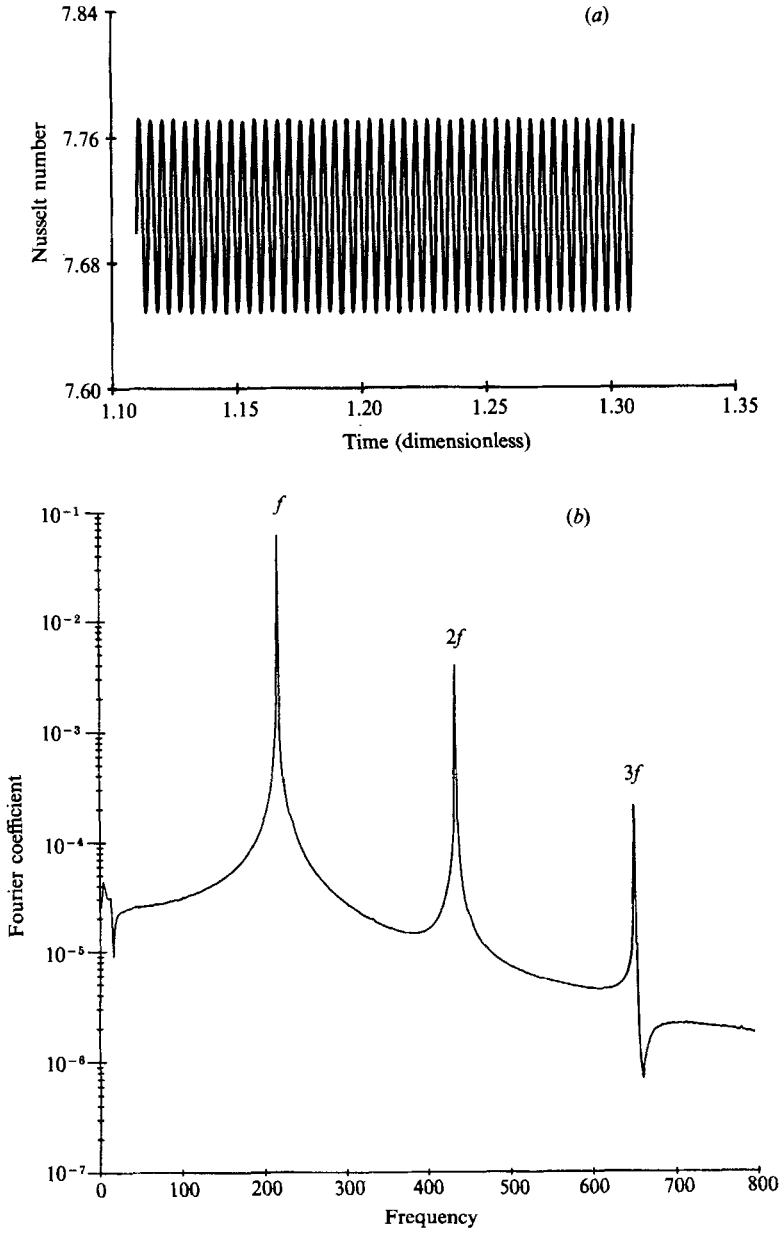

FIGURE 3. (*a*) Temporal variations in the Nusselt number and (*b*) the corresponding discrete Fourier transform for $R^* = 600$.

lines on the front face represent the temperature along vertical lines at the left edge, centre, and right edge of the cube face. The three sets of rectangular dashed lines enclosing the solid temperature lines mark the temperature range of zero to one from left to right. The solid line touches the left dashed line at the top and the right dashed line at the bottom, indicating that the non-dimensional temperature is zero and one at these surfaces respectively. The diagonally dashed line represents the linear conduction temperature profile that would exist if there were no convection present. The deviation of the solid line from the diagonally dashed line shows the effect of the

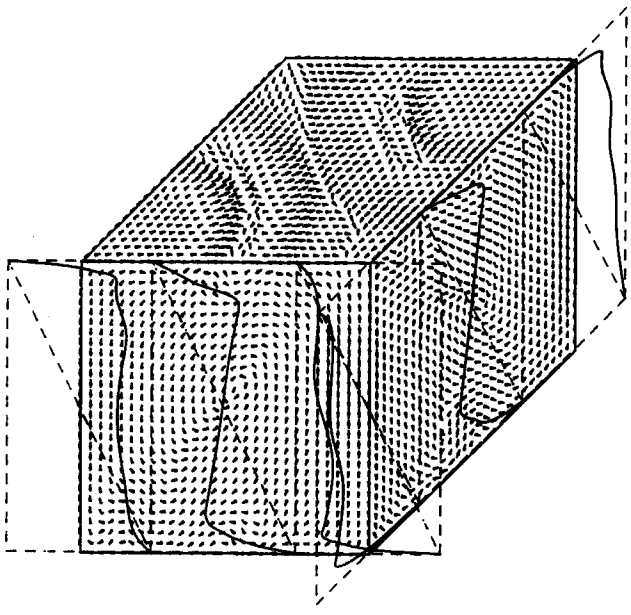

FIGURE 4. Typical velocity and temperature distributions at the boundaries of a cube with insulated vertical sides for $R^* = 800$ at the time $t = 0.152$. The grid size is $29 \times 29 \times 29$. Arrows represent velocity vectors and solid lines represent vertical temperature distributions at the centre and corners of the vertical sides.

convection. The clockwise flow on the front face of the cube produces temperatures larger than the conduction profile on the left edge since hot fluid from the bottom is convected upwards. Likewise temperatures smaller than the conduction profile are produced by cold fluid from the top convected downward. The solid and dashed lines on the other vertical side have the same meanings as on the front face. Note that the two solid lines at the front right edge are the same temperature with different perspective. The unsteady behaviour is characterized by locally hot or cold regions of fluid being carried by the main flow. This can be observed in figure 2 by the local variations in the vertical temperature distribution at the corners that is not characteristic of steady flows. A pictoral sequence showing nine time steps between successive Nusselt maxima indicates that there are at least four pairs of hot and cold regions being carried by the main stream for $R^* = 600$. This result has not been reported previously for rectangular boxes. However, Caltagirone (1975) observes four counter-rotating vortices varying around a mean position to coexist at high Rayleigh numbers in a rectangular cross-section of small aspect ratio. For slightly larger aspect ratios, four or eight additional rolls may appear. Caltagirone interprets these rolls as microvortices resulting from thermal instabilities near the sides.

The case $R^* = 600$ is used to demonstrate typical variations in the Nusselt number for the regularly fluctuating convection regime. Figure 3 shows the temporal variations in the Nusselt number and the corresponding discrete Fourier transform of this curve. The long-time solution is periodic with constant amplitude centred about a steady time-averaged Nusselt number. The discrete Fourier transform is shown as the magnitude of the Fourier coefficient plotted for each frequency. The three peaks correspond to the fundamental frequency of the periodic variation in the Nusselt number and its harmonics.

The fundamental frequency of the regularly fluctuating convection increases as the Rayleigh number increases. For $R^* = 560$, 580, 600, and 625, the frequency increases according to $f = 181$, 188, 216, and 260 (non-dimensional time)$^{-1}$, respectively. With these values, f is approximately proportional to $(R^*)^{3.6}$. The proportionality was determined using standard linear regression techniques.

The case of $R^* = 800$ is used to demonstrate typical flow patterns and temperature distributions for the irregularly fluctuating convection regime as shown in figure 4. Similar to the regularly fluctuating convection, locally hot and cold regions of fluid carried by the main flow are observed as local variations in the vertical temperature distribution at the corners. These local regions of fluid also correspond to the velocity surges moving towards the centre on the top face of the cube.

The nature of the fluctuations in the irregularly fluctuating convection regime is more complex than in the regularly fluctuating convection regime. For example, at $R^* = 650$, the fluctuations in the Nusselt number are composed of two basic frequencies. At this Rayleigh number, the four frequencies with the largest Fourier coefficient that can be identified from the Fourier transform of the Nusselt versus time curve are 150, 333, 483, and 656 (non-dimensional time)$^{-1}$. The third frequency is the sum of the first two and the fourth frequency is approximately the first harmonic of the second frequency. The transition from a periodic flow to a flow with two basic frequencies for fluctuating convection in a cube is similar to the transition Schubert & Straus (1982) observe in a square cross-section. The Fourier transforms for $R^* = 700$ and 800 show that the fluctuations are not composed of any distinct frequencies for the set of data analysed. The transforms exhibit characteristics similar to those Kimura, Schubert & Straus (1986) obtain for their non-periodic solutions in a square cross-section. Kimura *et al.* observe three states as the flow changes from steady to non-periodic: periodic, quasi-periodic or a flow with two basic frequencies, and a second periodic state. In the present study the following states are observed: a regular or periodic state, a state with two basic frequencies, and an irregular or non-periodic state.

3.2. *Natural convection in a cube with finite heat transfer on the vertical sides*

As an extension of the problem discussed in the previous section, the effect of finite heat transfer through the vertical sides instead of insulated sides is considered. Except for the change in boundary conditions on the vertical sides, all other conditions are the same. The heat transfer from the vertical sides is characterized by the Biot number, B^*, in the thermal boundary conditions (12)–(14). In all runs the ambient temperature T_∞ is set equal to the cold upper surface, the grid size is $N \times M \times P = 9 \times 9 \times 33$, and the initial conditions are values at the conduction state. Although a grid size of $11 \times 11 \times 41$ is used for the insulated case at $R^* = 300$, a grid size of $9 \times 9 \times 33$ is used for the finite heat transfer case at $R^* = 300$ to be consistent with the other R^* values. This should introduce little error since the difference in Nu at $R^* = 300$ is less than 0.3% between the two grid sizes. Distinct flow patterns are observed for increasing values of B^*.

The type of flow pattern observed depends on the Biot number as well as the Rayleigh number. In all cases three distinct patterns have been identified. As the Biot number increases for $R^* = 100$, the flow pattern changes from a unicellular three-dimensional pattern to a unicellular two-dimensional pattern and then to a different unicellular three-dimensional pattern as shown in figure 5(*a–c*). All figures illustrate typical flow patterns. As the Biot number increases for $R^* = 150$, 200, and 300, the flow pattern changes from a unicellular three-dimensional pattern to a

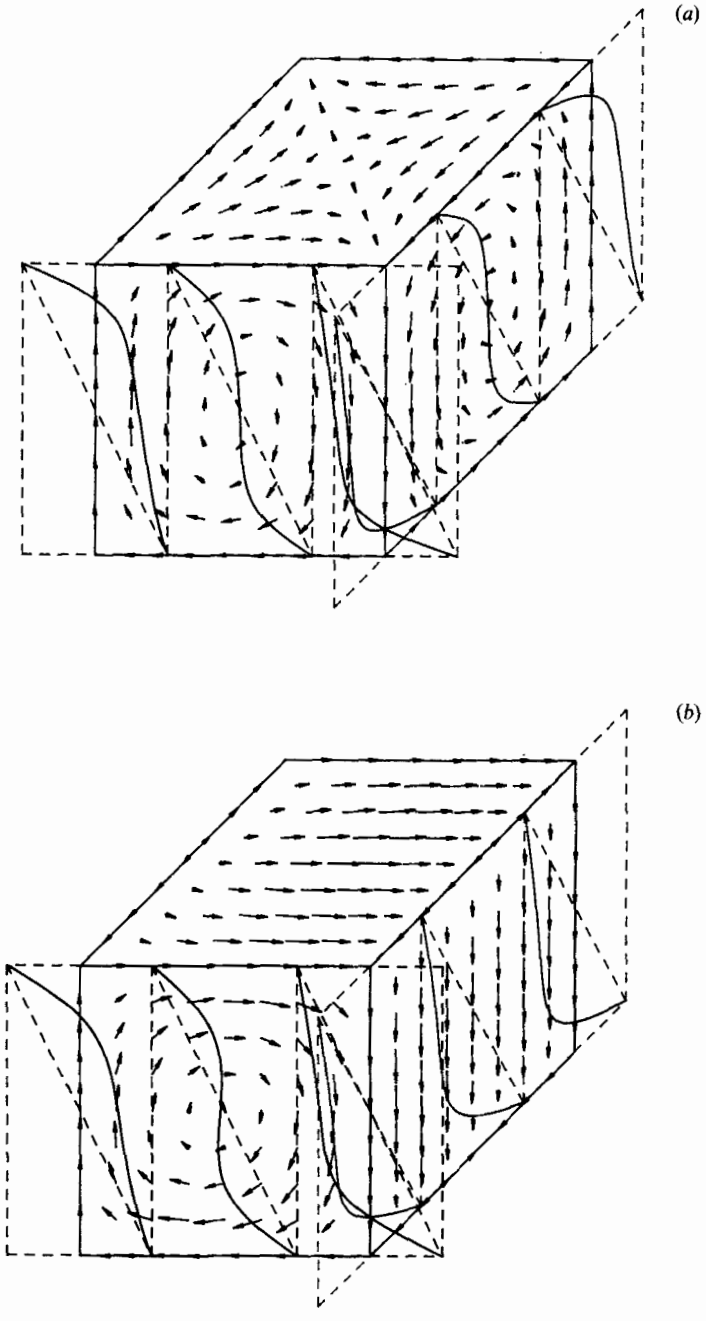

FIGURE 5(a, b). For caption see facing page.

bicellular two-dimensional pattern and then to a different unicellular three-dimensional pattern as shown in figure 6(a–c). Flow patterns for $R^* = 300$ in figure 6 are representative of similar patterns for $R^* = 150$ and 200. It is reasonable to assume that the bicellular roll will exist instead of the unicellular roll at larger Rayleigh numbers since both Schubert & Straus (1979) and Horne & O'Sullivan (1974) show that multicellular flows are steady at larger Rayleigh numbers when

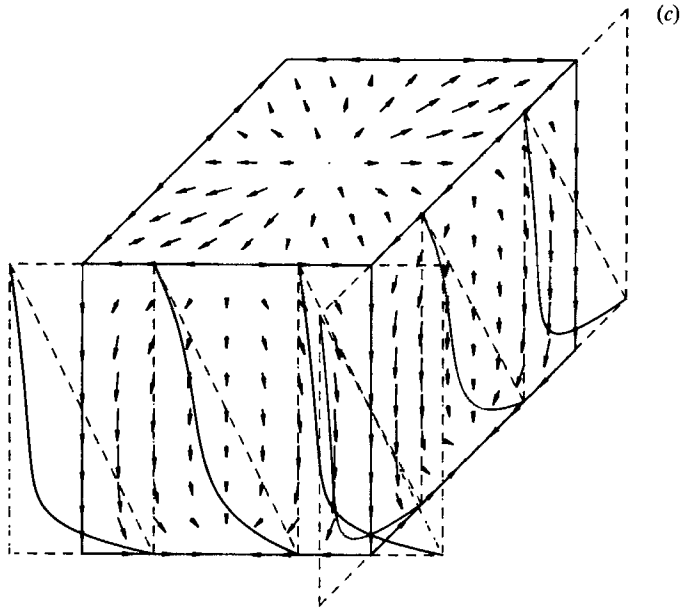

FIGURE 5. Velocity and temperature distributions for $R^* = 100$ and (*a*) $B^* = 0.160$, (*b*) 0.161, and (*c*) 2.00.

unicellular rolls are not. In all cases for $100 \leqslant R^* \leqslant 300$, the flow pattern shown in figures 5(*c*) and 6(*c*) appears most stable for large B^* since the fluid flows downward on all four vertical sides exposed to a cold ambient and up the centre. A similar phenomenon occurs for large B^* values when the ambient temperature is set equal to the hot lower surface. For this case, fluid flows upward on all four vertical sides exposed to a hot ambient and down the centre.

The Nu–B^* curve shown in figure 7 summarizes the nature of the motion for $B^* \leqslant 0.5$ in the range $150 \leqslant R^* \leqslant 300$. At small B^*, the unicellular three-dimensional motion consists of an ascending flow at diagonally opposed edges of the cube and a descending flow at the other diagonally opposed edges. This motion also exists in a cube with insulated vertical sides and the Nusselt numbers for the insulated case at $B^* = 0$ shown in figure 7 are the same values listed in table 1. The Nusselt number increases as the Biot number increases. This occurs because the Nusselt number, averaged over the bottom surface, accounts not only for the heat transfer through the top but also the increasing amount of heat transfer through the sides. The unicellular three-dimensional motion exists until a critical value of the Biot number, B^*_{cr}. At this value there is an abrupt decrease in the Nusselt number and an accompanying change in motion to the two-dimensional bicellular roll. Typical flow patterns for $150 \leqslant R^* \leqslant 300$ at B^*_{cr} are shown in figures 6(*a*, *b*) for $R^* = 300$. The flow also changes from three- to two-dimensional motion at B^*_{cr} for $R^* = 100$. Instead of the bicellular roll that exists for $150 \leqslant R^* \leqslant 300$, however, the flow is a unicellular roll for $R^* = 100$. The flow patterns at B^*_{cr} are shown in figure 5(*a*, *b*).

The critical values of B^* and the accompanying decrease in Nusselt number for $100 \leqslant R^* \leqslant 300$ are summarized in table 4. Although the variation in B^*_{cr} is not monotonic, it is not unreasonable to expect that this will occur since the flows are different for $R^* = 100$ and $150 \leqslant R^* \leqslant 300$. The transition to the two-dimensional

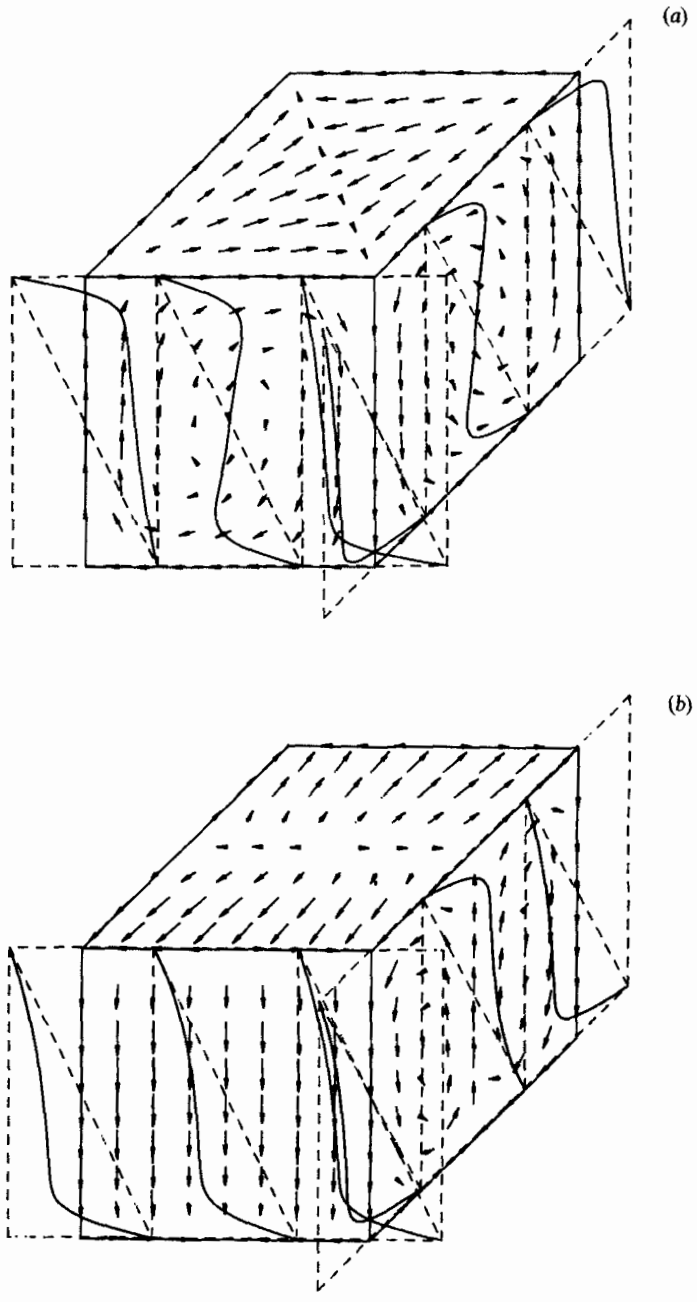

FIGURE 6(a, b). For caption see facing page.

bicellular roll for $150 \leqslant R^* \leqslant 300$ occurs at approximately the same critical value of B^*. To be consistent, a $9 \times 9 \times 33$ grid size was chosen to determine B^*_{cr} for all runs. It may be possible that the variation in B^*_{cr} will change with larger grid size. Results from preliminary work indicate that there is also an abrupt transition from the two-dimensional roll to the second three-dimensional motion.

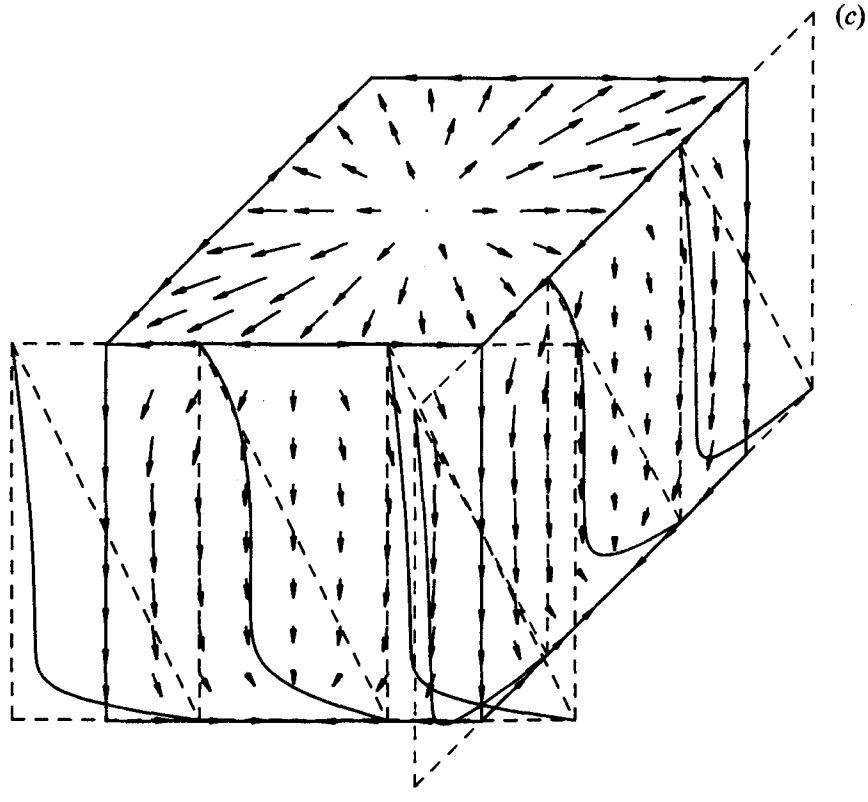

FIGURE 6. Velocity and temperature distributions for $R^* = 300$ and (*a*) $B^* = 0.103$, (*b*) 0.104, and (*c*) 2.00.

4. Summary and discussion

Natural convection in a cube of fluid-saturated porous medium has been studied numerically. In the first of the two special cases considered, the vertical sides of the cube are insulated and the range of Rayleigh numbers has been extended to 800. Between $550 < R^* < 560$, a transition from steady three-dimensional flow to regularly fluctuating three-dimensional flow is observed with a corresponding change in the slope of the Nusselt–Rayleigh number curve. The change in slope is consistent with the experimental observations of Combarnous (1970) for a horizontal layer. The regularly fluctuating flow is characterized by periodic oscillations in the Nusselt number and the frequency of these oscillations is found to vary approximately as $f \propto (R^*)^{3.6}$. This represents a relationship not determined previously for regularly fluctuating convection in a cube. However, Schubert & Straus (1982) determine for regularly fluctuating convection in a square cross-section that $f \propto (R^*)^n$ where $n = \frac{7}{8}$ or $\frac{3}{2}$ depending on the Rayleigh number. Horne & O'Sullivan (1978) attempt to explain the power $n = \frac{3}{2}$ using the mechanisms of instabilities in the thermal boundary layer and the circulation time. Preliminary attempts to explain the powers $n = \frac{7}{8}$ and 3.6 were not successful although power relations for other geometries, such as horizontal layers, may eventually prove useful in the attempt. Between $625 < R^* < 640$, a second transition from the regularly fluctuating flow to irregularly fluctuating flow is observed. At $R^* = 640$ and 650, for example, the fluctuations in

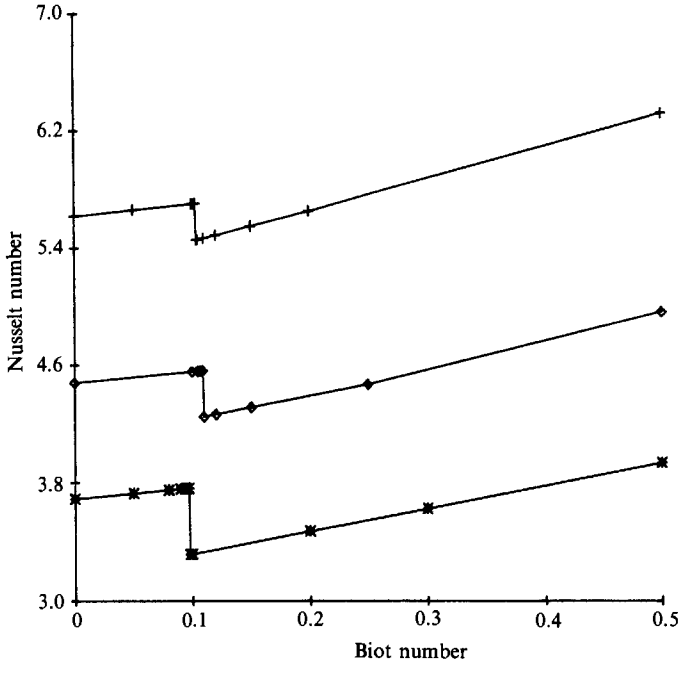

FIGURE 7. Variations in the Nusselt number with the Biot number for $R^* = 150$ (⊗), 200 (◇), and 300 (+).

Rayleigh number	B^*_{cr}	ΔNu
100	0.160	−0.064
150	0.097	−0.447
200	0.109	−0.317
300	0.103	−0.245

TABLE 4. Critical values of B^* for various Rayleigh numbers. B^*_{cr} and ΔNu are the critical value of B^* and accompanying decrease in Nu number at the first transition respectively.

the Nusselt number are composed of two basic frequencies. The transition from a periodic flow to a flow with two basic frequencies has not been reported for a cube; however, this transition is similar to the one Schubert & Straus (1982) observe in a square cross-section. For $R^* = 700$ and 800 the fluctuations in the Nusselt number are not composed of any distinct frequencies. Although the values of R^* at which the transitions to regularly and irregularly fluctuating convection occur are larger than the values Schubert & Straus (1979) observe, the nature of the flow at each transition is quite similar. These transitions are also similar to the experimental observations of Seki *et al.* (1980) for a horizontal layer.

In the second case, finite heat transfer through the vertical sides of the cube is considered. The numerical results indicate the existence of three distinct flow patterns depending on heat transfer characterized by a Rayleigh number and a Biot number appropriate for porous medium. At small Biot numbers, the motion is three-dimensional and consists of an ascending flow at diagonally opposed edges of the cube and a descending flow at the other diagonally opposed edges. As the Biot

number increases, the motion changes to a two-dimensional flow having either one or two cells depending on the Rayleigh number and then to a different three-dimensional motion involving a descending flow on all vertical sides and an ascending flow at the centre. The transition from the first to the second flow pattern occurs abruptly at a critical Biot number for all Rayleigh numbers. The value for the critical Biot number is approximately the same for two-dimensional flows with bicellular rolls.

The authors gratefully acknowledge resources from the Nuclear Technology and Applications Development Department at Sandia National Laboratories, Albuquerque, to complete the numerical calculations.

REFERENCES

BECK, J. L. 1972 Convection in a box of porous material saturated with fluid. *Phys. Fluids* **15**, 1377.

BURETTA, R. J. & BERMAN, A. S. 1976 Convective heat transfer in a liquid-saturated porous layer. *Trans. ASME* E: *J. Appl. Mech.* **98**, 249.

CALTAGIRONE, J.-P. 1975 Thermoconvective instabilities in a horizontal porous layer. *J. Fluid Mech.* **72**, 269.

CALTAGIRONE, J.-P. 1976 Thermoconvective instabilities in a porous medium bounded by two concentric horizontal cylinders. *J. Fluid Mech.* **76**, 337.

CALTAGIRONE, J.-P., CLOUPEAU, M. & COMBARNOUS, M. 1971 Convection naturelle fluctuante dans une couche poreuse horizontale. *C R Acad. Sci. Paris* B**273**, 833.

COMBARNOUS, M. 1970 Convection naturelle et convection mixte dans une couche poreuse horizontale. *Revue Gén. Thermique* **108**, 1355.

COMBARNOUS, M. & LEFUR, B. 1969 Transfert de chaleur par convection naturelle dans une couche poreuse horizontale. *C R Acad. Sci. Paris* B**269**, 1009.

GARY, J. & KASSOY, D. R. 1981 Computation of steady and oscillatory convection in saturated porous media. *J. Comput. Phys.* **40**, 120.

GUPTA, V. P. & JOSEPH, D. D. 1973 Bounds for heat transport in a porous layer. *J. Fluid Mech.* **57**, 491.

HIRASAKI, G. J. & HELLUMS, J. D. 1968 A general formulation of the boundary conditions on the vector potential in three-dimensional hydrodynamics. *Q. J. Appl. Maths* **26**, 331.

HOLST, P. H. & AZIZ, K. 1972 Transient three-dimensional natural convection in confined porous media. *Intl J. Heat Mass Transfer* **15**, 73.

HORNE, R. N. 1979 Three-dimensional natural convection in a confined porous medium heated from below. *J. Fluid Mech.* **92**, 751.

HORNE, R. N. & O'SULLIVAN, J. M. 1974 Oscillatory convection in a porous medium heated from below. *J. Fluid Mech.* **66**, 339.

HORNE, R. N. & O'SULLIVAN, J. M. 1978 Origin of oscillatory convection in a porous medium heated from below. *Phys. Fluids* **21**, 1260.

KASSOY, D. R. & COTTE, B. 1985 The effect of sidewall heat loss on convection in a saturated porous vertical slab. *J. Fluid Mech.* **152**, 361.

KIMURA, S., SCHUBERT, G. & STRAUS, J. M. 1986 Route to chaos in porous-medium thermal convection. *J. Fluid Mech.* **166**, 305.

LOWELL, R. P. & HERNANDEZ, H. 1982 Finite amplitude convection in a porous container with fault-like geometry: effect of initial and boundary conditions. *Intl J. Heat Mass Transfer* **25**, 631.

MALKUS, W. V. R. 1954 The heat transport and spectrum of thermal turbulance. *Proc. R. Soc. Lond.* A**225**, 196.

PLATZMAN, G. W. 1965 The spectral dynamics of laminar convection. *J. Fluid Mech.* **23**, 481.

RIAHI, N. 1983 Nonlinear convection in a porous layer with finite conducting boundaries. *J. Fluid Mech.* **129**, 153.

ROACHE, P. 1972 *Computational Fluid Dynamics*, Chap. 3. Albuquerque: Hermosa.

SCHUBERT, G. & STRAUS, J. M. 1979 Three-dimensional and multicellular steady and unsteady convection in fluid-saturated porous media at high Rayleigh numbers. *J. Fluid Mech.* **94**, 25.

SCHUBERT, G. & STRAUS, J. M. 1982 Transitions in time-dependent thermal convection in fluid-saturated porous media. *J. Fluid Mech.* **121**, 301.

SEKI, N., FUKUSAKO, S. & ARIAKE, Y. 1980 Experimental study of free convective heat transfer in a liquid-saturated porous bed at high Rayleigh number. *Warme- und Stoffubertragung* **13**, 61.

STAMPS, D. W. 1985 Thermal instabilities in porous media. Ph.D. thesis, University of Michigan.

STAMPS, D. W. & CLARK, J. A. 1986 Unsteady thermocline degradation in a fluid-saturated, porous medium. *Intl J. Heat Mass Transfer* **29**, 1063.

STEEN, P. H. 1983 Pattern selection for finite-amplitude convection states in boxes of porous media. *J. Fluid Mech.* **136**, 219.

STRAUS, J. M. & SCHUBERT, G. 1979 Three-dimensional convection in a cubic box of fluid-saturated porous material. *J. Fluid Mech.* **91**, 155.

WEIDMAN, P. D. & KASSOY, D. R. 1986 The influence of side wall heat transfer on convection in a confined saturated porous medium. *Phys. Fluids* **29**, 349.